JACS JOURNAL OF THE AMERICAN CHEMICAL SOCIETY

Article

Cite This: J. Am. Chem. Soc. 2019, 141, 19389−19396

pubs.acs.org/JACS

Azulene-Derived Fluorescent Probe for Bioimaging: Detection of Reactive Oxygen and Nitrogen Species by Two-Photon Microscopy

Lloyd C. Murfin,[†,#] Maria Weber,[†,‡,#] Sang Jun Park,[§,#] Won Tae Kim,[§,#] Carlos M. Lopez-Alled,[†,‡] Claire L. McMullin,[†] Fabienne Pradaux-Caggiano,[†] Catherine L. Lyall,[∥] Gabriele Kociok-Köhn,[∥] Jannis Wenk,[‡,⊥] Steven D. Bull,[†,‡] Juyoung Yoon,[▽] Hwan Myung Kim,[*,§] Tony D. James,[*,†,‡] and Simon E. Lewis[*,†,‡]

[†]Department of Chemistry, University of Bath, Bath BA2 7AY, United Kingdom

[‡]Center for Sustainable Circular Technologies, University of Bath, Bath BA2 7AY, United Kingdom

[§]Department of Energy Systems Research, Ajou University, Suwon 443-749, South Korea

[∥]Materials and Chemical Characterization (MC^2), University of Bath, Bath BA2 7AY, United Kingdom

[⊥]Department of Chemical Engineering, University of Bath, Bath BA2 7AY, United Kingdom

[▽]Department of Chemistry and Nano Science, Ewha Woman's University, Seoul 120-750, South Korea

Supporting Information

ABSTRACT: Two-photon fluorescence microscopy has become an indispensable technique for cellular imaging. Whereas most two-photon fluorescent probes rely on well-known fluorophores, here we report a new fluorophore for bioimaging, namely azulene. A chemodosimeter, comprising a boronate ester receptor motif conjugated to an appropriately substituted azulene, is shown to be an effective two-photon fluorescent probe for reactive oxygen species, showing good cell penetration, high selectivity for peroxynitrite, no cytotoxicity, and excellent photostability.

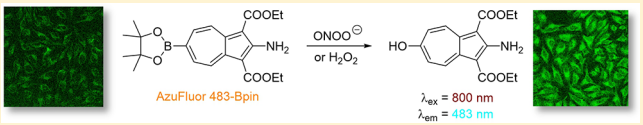

INTRODUCTION

Reactive oxygen species (ROS) and reactive nitrogen species (RNS) are important mediators in many physiological and pathological processes.[1] The one-electron reduction of O_2 *in vivo* leads to the formation of $O_2^{\bullet-}$ (superoxide), which in turn undergoes disproportionation catalyzed by superoxide dismutase to give O_2 and H_2O_2 (hydrogen peroxide). Another fate of $O_2^{\bullet-}$ is to react with endogenously produced NO (nitric oxide) to form $ONOO^-$ (peroxynitrite) via a nonenzymatic process. Ordinarily, the flux of H_2O_2 is tightly regulated; aberrant H_2O_2 production or overexposure is implicated in the pathogenesis of many diseases such as cancer and neurodegenerative conditions.[2] Similarly, while $ONOO^-$ has roles in signal transduction, its strongly oxidizing and nitrating properties mean it can react in an uncontrolled manner with various biomolecules.[3] Elevated levels of $ONOO^-$ have been linked to cardiovascular, neurodegenerative, and inflammatory diseases as well as cancer.[4] In view of this, there is a significant need for tools and techniques to elucidate the roles of $ONOO^-$, H_2O_2, and other ROS/RNS in biological systems.

Of the various techniques that have been employed for the study of ROS/RNS, the use of fluorescent probes has several advantages. They can enable realtime fluorescence imaging of ROS/RNS with high sensitivity, are nondestructive, and are usually operationally straightforward. Such fluorescent probes may be categorized as chemosensors (those which reversibly bind their analytes) and chemodosimeters (irreversible reaction-based probes). Probes of this second type often have high analyte selectivity and are applicable even to those ROS/RNS that have very short lifetimes.[5] We and others have reported many fluorescent probes for imaging ROS/RNS,[6] including H_2O_2[7] and $ONOO^-$.[8] In the field of fluorescence imaging, the use of two-photon excitation fluorescence microscopy (TPM)[9] brings particular advantages. Specifically, TPM allows higher spatial resolution, and the use of excitation wavelengths in the near-infrared (NIR) region allows much greater tissue penetration, since minimal absorption by hemoglobin and water occurs in the NIR window.[10] Furthermore, excitation by lower energy photons means photobleaching and damage to the sample are minimized, and the autofluorescence of intrinsic fluorophores is avoided.[11]

The design and development of small-molecule based fluorescent probes that can be used in TPM has been an area of much recent research activity.[12] Among these, various two-photon fluorescent probes for ROS/RNS have been exploited, since one-photon excitation with short wavelength could generate artificial ROS/RNS.[13] For H_2O_2, two-photon fluorescent probes have been reported that utilize the reaction with boronic acids or their esters, with nitroxide radicals, or Baeyer−Villiger type rearrangements.[14] For $ONOO^-$, two-photon fluorescent probes have been reported that also utilize

Received: September 10, 2019
Published: November 27, 2019

DOI: 10.1021/jacs.9b09813
J. Am. Chem. Soc. 2019, 141, 19389−19396

the reaction with boronic acids or their esters, as well as ones which function by oxidation of electron-rich arenes, α-ketocarbonyls, selenides, or by nucleophilic addition to electron-poor alkenes and arenes.[15] These reported probes incorporate a variety of fluorophores, including well-known ones that have been extensively used in one-photon fluorescence, such as naphthalimides, rhodamines, coumarins, etc. In contrast, in the work presented here, we report a fluorescent probe for ROS/RNS that incorporates a previously unexploited class of fluorophore, namely an azulene.

Azulene is a nonalternant bicyclic aromatic hydrocarbon, isomeric with naphthalene, yet with appreciably different properties.[16] The $S_0 - S_1$ energy gap is smaller than in naphthalene, leading to an absorption in the visible region, and hence the blue color for which azulene is named. The nonradiative $S_1 \rightarrow S_0$ transition is extremely fast,[17] whereas the nonradiative $S_2 \rightarrow S_1$ transition is much slower.[18] Consequently, $S_2 \rightarrow S_0$ fluorescence is the principal mode of emission,[19] in violation of Kasha's rule.[20] The predominance of emission from higher excited states has also been noted for many azulene derivatives.[21] These properties have led to azulenes being used extensively as both colorimetric[22] and fluorescent[23] probes for various analytes. Azulene derivatives have also been exploited as fluorescence sensitizers[24] and quenchers[25] as well as in photoswitches[26] and molecular logic gates.[27] In the context of bioimaging, ^{18}F-labeled azulene derivatives have been used for PET imaging,[28] but to our knowledge, azulenes have not previously been used for fluorescence imaging. In the specific context of ROS/RNS detection, no reports employing azulene-containing probes have appeared to date. The two-photon fluorescence of azulene[29] and some derivatives[30] has been studied, yet it has never been utilized in any sensing context (although it has been exploited for fluorescence lithography[31] and applications in optical data storage have been suggested[32]).

RESULTS AND DISCUSSION

Design Principles. Our design strategy for an azulene chemodosimeter imaging probe is centered on the concept of an inversion of internal charge transfer (ICT) directionality upon reaction with the analyte. This exploits the inherent dipole moment of azulene of 1.08 D, unusually high for a hydrocarbon. Thus, the charge distribution in azulene is as shown in Scheme 1a, with the smaller ring having the higher electron density as a result of the contribution of the resonance structure shown, in which both rings (tropylium and cyclopentadienide) are discrete 6π aromatic systems. Our approach involves the use of a pinacol boronate ester as a receptor motif, whose reaction with ROS/RNS leads to the desired reversal of the direction of ICT. In many cases, boronate-based probes function by the carbon−boron bond undergoing oxidation by the ROS/RNS to give a carbon−oxygen bond, which in turn leads to the cleavage of a self-immolative linker and a change in fluorescence response. In the present case, we reasoned that a boronate group appended directly to the azulene seven-membered ring could effect the desired perturbation of the fluorophore upon reaction with ROS/RNS (Scheme 1b). This approach exploits the fact that the boronic ester is electron-withdrawing (Scheme 1c), whereas the hydroxyl group is electron-donating by resonance (Scheme 1d). Our strategy anticipates that the electronic influence of the boronic ester will attenuate the inherent polarization of the azulene, leading to the Az-6-Bpin system having reduced ICT character overall. On the other hand, the effect of the hydroxyl group in the Az-6-OH system will reinforce the inherent polarization of the fluorophore, and hence lead to increased ICT character overall and enhanced fluorescence.

Scheme 1. Initial Concept for Azulene-Based Fluorescent Probe for ROS/RNS

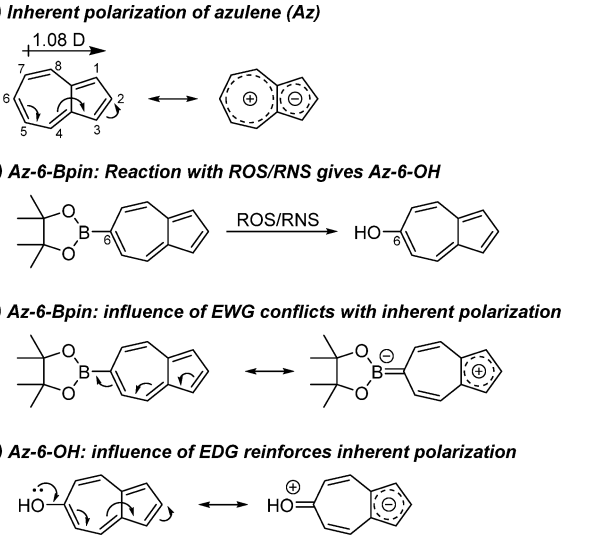

The simplest embodiment of the design strategy described above would be to synthesize and evaluate 6-azulenyl pinacolborane itself as a fluorescent probe. However, the reaction product, 6-hydroxyazulene, is reportedly unstable, which may be due in part to the fact that it exists in tautomeric equilibrium with its keto form.[33] We therefore refined our design strategy, introducing esters at the azulene 1- and 3-positions, as this substitution pattern is known to stabilize 6-hydroxyazulenic compounds.[34] Finally, we introduced an electron-donating group (amine) at the 2-position. The final probe structure **1** and its oxidation product **2** are depicted in Scheme 2a. The purpose of the amine substituent is to enhance the contribution of the resonance effect that conflicts with the inherent polarity of azulene, as shown in Scheme 2b, with an additional ammonium-boronate resonance contribution compared to Scheme 1c. Furthermore, the ester groups will not only stabilize the hydroxyazulene product **2** of reaction with ROS/RNS, they will also enhance the contribution of the resonance effect that reinforces the inherent polarity of azulene, as shown in Scheme 2c.

Probe molecule **1** and its oxidation product **2** were modeled using DFT as well as azulene itself. NBOs (natural bonding orbitals) were computed, and selected molecular orbitals (HOMO, LUMO, and LUMO+1) for each compound are shown in Figure 1.

The probe molecule **1** may be accessed in three steps from commercial materials (see ESI).[35] We have termed this substance "AzuFluor 483-Bpin" (to indicate the nature of the receptor motif and the emission maximum of its turn-on response). AzuFluor **1** was then reacted with H_2O_2 (THF, 24 h, 95%) and the novel product isolated and fully characterized as the stable 6-hydroxyazulene **2**. Crystals of **2** suitable for X-ray diffraction were grown from THF/hexane and the solid state structure of **2** is shown in Figure 2.

Probe Characterization. The AzuFluor probe **1** itself exhibits near-negligible fluorescence, whereas the oxidation

DOI: 10.1021/jacs.9b09813
J. Am. Chem. Soc. 2019, 141, 19389−19396

Scheme 2. Final Sensor Design for Azulene-Based Fluorescent Probe for ROS/RNS

a) AzuFluor 483-Bpin: Reaction with ROS/RNS

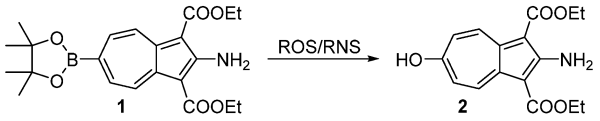

b) Influence of Bpin and amine groups conflicts with inherent polarization to a greater extent

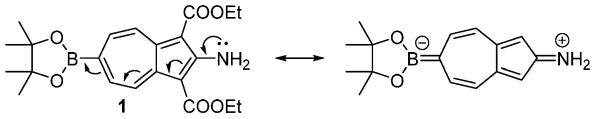

c) Influence of hydroxyl and ester groups reinforces inherent polarization to a greater extent

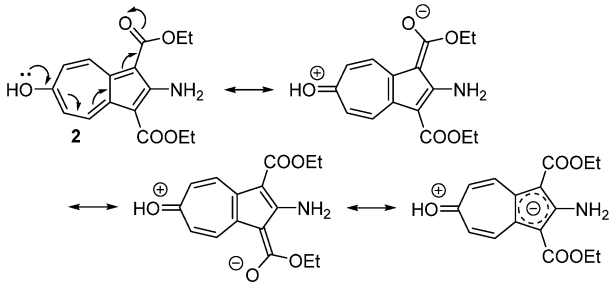

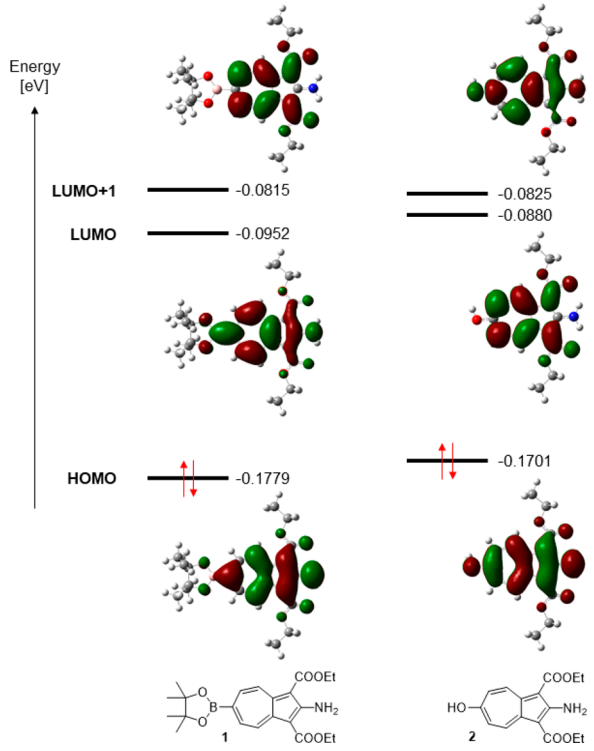

Figure 1. Selected molecular orbitals for azulene (left), 1 (center) and 2 (right). DFT calculations used the BP86 functional and 6-31G** basis set; see ESI for full details.

product **2** exhibits fluorescence emission at λ_{em} = 483 nm, upon excitation at 350 nm, in a mixed aqueous buffer/methanol system, as shown in Figure 3. Fluorescence excitation spectra were also acquired (Figures S1–S3), as well as UV–vis absorption spectra (Figure S4). A value of λ_{max} = 335 nm was

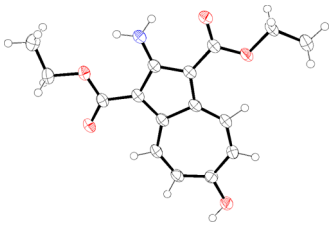

Figure 2. Solid state structure of **2**. Ellipsoids are represented at 50% probability. H atoms are shown as spheres of arbitrary radius. CCDC 1899490.

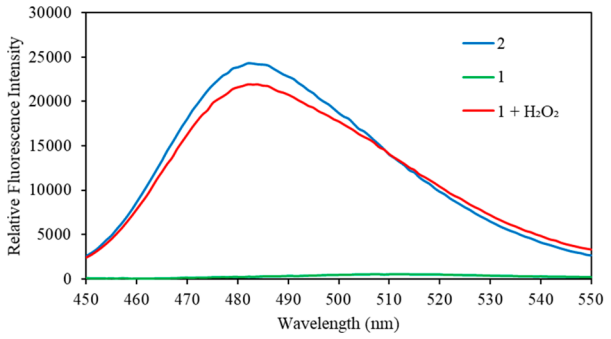

Figure 3. Comparison of one-photon fluorescence emission spectrum of **1** with **2**. Emission spectrum of **2** (500 nM) and **1** (500 nM) with and without H_2O_2 (200 μM) in PBS buffer 52% H_2O: MeOH, pH 8.2 at 25 °C. Fluorescence intensities were measured with λ_{ex} = 350 (bandwidth: 20) nm on a BMG Labtech CLARIOstar plate reader.

observed in the absorption spectrum of **2**; thus, the oxidation product displays an appreciable Stokes shift of 148 nm. Fluorescence emission of **2** was also examined in various solvents (Figure S5), and we observed the solvatofluorochromism expected for an ICT fluorophore; the observed λ_{em} value underwent a bathochromic shift from 480 to 491 nm with increasing solvent polarity.

A pH titration showed that the fluorescence intensity is greatest at pH 7–8 (Figure 4; see also Figures S6–S8), which

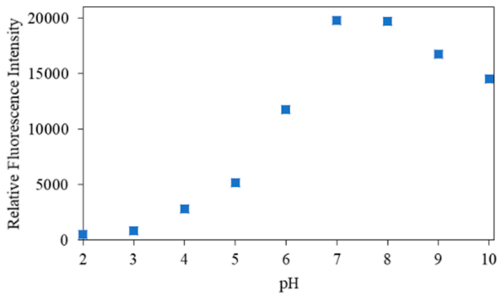

Figure 4. Effect of various pH on fluorescence intensity of **2** (500 nM) in 52% MeOH: 48% 0.1 M NaCl with λ_{max} = 483 nm.

corresponds to the pH range at which a probe for cellular imaging would need to function in most cases. Fluorescence intensity decreases markedly at lower pH, and is also attenuated above pH 8. An NMR study of **2** at different pH values (Figures S9–S11) shows it to be stable upon prolonged standing in solution across a range of pH values, albeit with a downfield shift of the aryl resonances at low pH. Thus, we do not believe the decrease in fluorescence at extremes of pH is due to decomposition of **2**. Rather, we ascribe these phenomena to changes in the ionization state of **2**. Thus, at

DOI: 10.1021/jacs.9b09813
J. Am. Chem. Soc. 2019, 141, 19389–19396

low pH the amino group in **2** would be protonated; in $[\mathbf{2}+H]^+$ the ICT interaction between the amine and the esters would be abolished. Conversely, at high pH, deprotonation of the aryl hydroxyl group to give $[\mathbf{2}\text{-}H]^-$ would also affect the fluorescence response. The computed pK_a values for the amine and hydroxyl groups in **2** are 3.60 and 10.95, respectively (Figures S12–S13), which supports the above explanation.

It is well established in the literature[14,15] that boronate receptors respond to both $ONOO^-$ and H_2O_2, although the greater nucleophilicity of $ONOO^-$ leads to a reaction rate $\sim 10^6$ greater than for H_2O_2.[36] We therefore evaluated **1** as a probe for both potential analytes, with the expectation of a faster and more sensitive response to peroxynitrite. Fluorescence titration experiments (Figure S14) with **1** and H_2O_2 established the limit of detection to be 1.72 μM. A time drive experiment (Figure S15) showed the fluorescence response of **1** (500 nM) to H_2O_2 to be slow, with fluorescence intensity continuing to increase after 30 min even at $[H_2O_2]$ = 500 μM. In contrast, **1** was much more sensitive to $ONOO^-$ as expected, with fluorescence titration experiments (Figure S16) establishing the limit of detection to be 21.7 nM. The selectivity of **1** for various ROS was then examined, and **1** was found to be highly selective for $ONOO^-$ and H_2O_2 over HOCl, $HO^\bullet$, $O_2^{\bullet-}$, $ROO^\bullet$, and $^1O_2$ (Figure S17). Furthermore, with equimolar concentrations of all ROS, **1** exhibited pronounced selectivity for $ONOO^-$ over H_2O_2 at both 5 and 30 min time points (Figures 5, S18–S19). The UV–vis spectroscopic response of **1** to $ONOO^-$ and H_2O_2 was also studied (Figures S20–S25; Tables S1–S2).

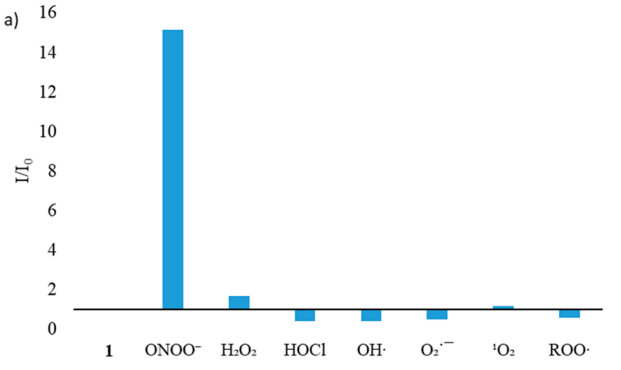

Figure 5. Selectivity data for **1** (500 nM) in the presence of $ONOO^-$, H_2O_2, HOCl, $OH^\bullet$, $O_2^{\bullet-}$, $^1O_2$, and $ROO^\bullet$ (each 500 nM). Data acquired 5 min after mixing, in PBS buffer 52% H_2O: MeOH, pH 8.2 at 25 °C, at λ_{max} = 483 nm. Fluorescence intensities were measured with λ_{ex} = 350 (bandwidth 20) nm, on a BMG Labtech CLARIOstar plate reader.

Two-photon action spectra ($\Phi\delta$, where Φ is the fluorescence quantum yield and δ is the two-photon absorption cross-section) of probe **1** in the presence and absence of H_2O_2 or $ONOO^-$ were investigated (Figure S26) to determine the maximum optical brightness. Upon addition of ROS, the spectroscopic maximum ($\Phi\delta_{max}$) was red-shifted from 700 to 810 nm, along with an increase of the $\Phi\delta$ value (at 810 nm) from 1.2 to 3.2 GM. A similar result was observed with two-photon microscopy imaging (Figure S27). The measured maximum two-photon optical brightness of $\Phi\delta_{max}$ = 3.2 GM compares favorably with the reported values[37] for other commonly used fluorophores of similar or greater molecular weight, such as dansyl hydrazine, Lucifer yellow, Cascade blue, or Indo-1 (see SI, Table S3 for a tabulated comparison). The fluorescence quantum yield of **2** was determined to be 0.010 (Figures S34–S36). Thus, at 810 nm the two-photon absorption cross-section of **2** ($\Phi\delta \div \Phi$) is 320 GM.

Probe Evaluation in Cell Studies. *In vitro* studies were performed to validate the ability of **1** in aqueous solution to detect endogenous and exogenous H_2O_2 and $ONOO^-$ by TPM. MTT assays confirmed that **1** is not cytotoxic under the identified imaging conditions (Figure S28). Two-photon excited fluorescence intensities were determined by staining HeLa cells with **1** at a concentration of 5 μM (by adding 5 μL of a 1 mM DMSO stock solution of **1** per 1 mL of total volume of medium) in the presence and then absence of $ONOO^-$ (100 μM), to find the optimal two-photon excitation wavelength (Figure S27a). This was determined to be λ_{ex} = 800 nm, at which wavelength the mean fluorescence intensity was nearly 4-fold higher after treatment with $ONOO^-$ (Figure S27b). Probe **1** showed high photostability, without any decay of fluorescence intensity even after irradiation for 1 h at 2 s intervals, both with and without pretreatment with $ONOO^-$ (Figure S29). Co-localization experiments were performed with **1** and representative organelle markers (ER, mitochondria, and lysosomes). The Pearson correlation coefficients with the markers for the ER, mitochondria and lysosomes are 0.79, 0.70 and 0.41, respectively (Figure S30). This indicates that **1** is distributed through the cytosol, including in these organelles, rather than any specific localization.

With ideal imaging conditions established, the ability of **1** to detect ROS in living cells was then demonstrated. Thus, the mean fluorescence intensity was measured for TPM images of **1** in RAW 264.7 macrophages pretreated with H_2O_2 (2 mM) and $ONOO^-$ (100 μM). The fluorescence intensity of cells pretreated with ROS was shown to increase nearly 3-fold (Figure 6b-c), compared to negative control (Figure 6a, cells stained with probe **1** only). Next, RAW 264.7 macrophages were pretreated with endogenous ROS-inducing reagents to observe whether probe **1** could respond to the endogenous ROS of macrophages. Phorbol myristate acetate (PMA),[38] and lipopolysaccharide/gamma interferon (LPS/IFN-γ)[39] are known to stimulate macrophages to release ROS such as $NO^\bullet$, $O_2^{\bullet-}$, H_2O_2, and $ONOO^-$, whereas 3-morpholinosydnonimine (SIN-1)[40] is employed as a positive control (exogenous source of $ONOO^-$). Each cell was individually incubated with either PMA (1 μg mL^{-1}), LPS (1 μg mL^{-1}) + IFN-γ (50 ng mL^{-1}), or SIN-1 (50 μM) and then stained with probe **1**. As a result, **1** showed strong fluorescence intensity, increasing by approximately 2-fold, as compared with the control group (Figure 6d,e,g). ROS-induced fluorescence intensity did not rise above basal levels upon cotreatment with ebselen (50 μM), a commonly used scavenger of superoxide (the precursor of $ONOO^-$ and H_2O_2;[41] Figure 6f,h). Overall, the obtained outcomes showed that **1** can directly detect the presence of H_2O_2 and $ONOO^-$ in biological systems.

Finally, we investigated the ability of probe **1** to visualize $ONOO^-$ and H_2O_2 in living tissues. A fresh slice of rat hippocampus was stained with **1** at a concentration of 50 μM (by adding 5 μL of a 10 mM DMSO stock solution of **1** per 1 mL total volume) for 1 h at 37 °C. The TPM images obtained in the CA1 regions displayed only weak signals, as we observed in cultured cells (Figure 7a,e). However, bright fluorescence was observed upon pretreatment with PMA (10 μg mL^{-1}) and SIN-1 (200 μM), increased by approximately 2 times

DOI: 10.1021/jacs.9b09813
J. Am. Chem. Soc. 2019, 141, 19389–19396

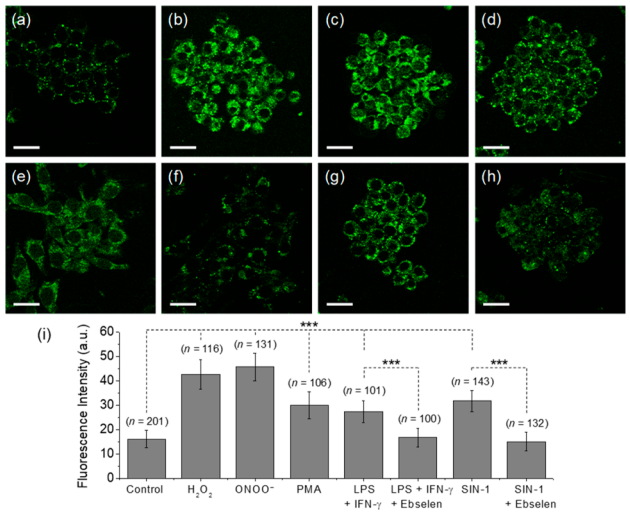

Figure 6. TPM images of RAW 264.7 macrophages stained with **1** (5 μM, 30 min). (a) Control image. (b–h) Cells were pretreated with (b) exogenous added H_2O_2 (2 mM, 30 min), (c) exogenous added $ONOO^-$ (100 μM, 30 min), (d) PMA (1 μg mL^{-1}, 30 min), (e) LPS (1 μg mL^{-1}, 4 h) and IFN-γ (50 ng mL^{-1}, 1 h), (f) LPS, IFN-γ and ebselen (50 μM, 30 min), (g) SIN-1 (50 μM, 30 min), and (h) SIN-1 and ebselen. (i) Average fluorescence intensity in the corresponding TPM images. Images were obtained using 800 nm as the excitation wavelength and 400–600 nm emission windows. Scale bars = 20 μm. Asterisks represent statistical significance (***$p < 0.001$) and n is the number of counted cells.

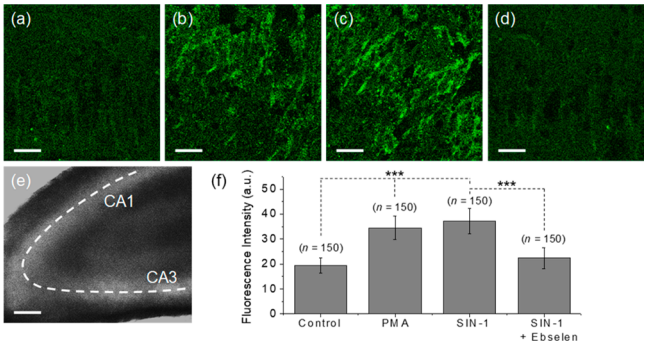

Figure 7. TPM images of rat hippocampal slices stained with **1** (50 μM, 1 h). (a) Control image. (b–d) Tissues were pretreated with (b) PMA (10 μg mL^{-1}, 30 min), (c) SIN-1 (200 μM, 30 min), and (d) SIN-1 and ebselen (each 200 μM, 30 min). (e) Bright-field image of the CA1 and CA3 regions of rat hippocampal slices. (f) Average fluorescence intensity in the corresponding TPM images. Images were obtained in the CA1 layer using 800 nm as the excitation wavelength and 400–600 nm emission windows. Scale bars = 25 (a–d) and 250 μm (e). Asterisks represent statistical significance (***$p < 0.001$) and n is the number of ROI from three samples for each imaging condition.

compared to negative control (Figure 7b,c) whereas fluorescence did not increase above basal levels upon cotreatment with SIN-1 and ebselen (200 μM) (Figure 7d,f). This confirms that our probe can directly detect endogenous ROS in living tissues with TPM.

CONCLUSIONS

We have synthesized and evaluated the first two-photon fluorescent bioimaging probe containing an azulene fluorophore. The rationally designed probe, AzuFluor 483-Bpin (**1**), has been shown to possess high selectivity for peroxynitrite and hydrogen peroxide over other reactive oxygen species. Furthermore, **1** is cell-permeable, photostable, and non-cytotoxic *in vitro* on the time scale of the two-photon fluorescence microscopy experiments. In view of the susceptibility of the azulene fluorophore to perturbation by attached substituents, the wide array of known receptor motifs that could be attached, and the availability of synthetic methodology to attach them, we anticipate that azulene fluorophores based on the design principles we have described here will find many further applications in two-photon fluorescence imaging.

EXPERIMENTAL SECTION

Preparation of Diethyl 2-amino-6-hydroxyazulene-1,3-dicarboxylate (2). Diethyl 2-amino-6-(4,4,5,5-tetramethyl-1,3,2-dioxaborolan-2-yl)azulene-1,3-dicarboxylate **1**[35] (100 mg, 0.24 mmol, 1.00 equiv) was dissolved in THF (2.5 mL) to which 30% aq. H_2O_2 solution (50 μL, 0.48 mmol, 2.0 equiv) was added. The bright-orange solution was left to stir in air for 24 h, affording a pale-yellow solution, after which water (10 mL) was added. The mixture was extracted with CH_2Cl_2 (2 × 20 mL), and the combined organic extracts were dried over $MgSO_4$ and then filtered. The filtrate was concentrated under reduced pressure, then the crude material was purified via silica column chromatography, eluting with EtOAc/Petrol (1:4 → 2:3) to afford **2** as an orange powder (70 mg, 95%). R_f = 0.16 (EtOAc/Petrol 1:4); m. pt. 117 °C (dec.); δ_H (500 MHz, $(CD_3)_2SO$) 11.02 (1H, s, OH), 8.99 (2H, dt, J 11.6, 1.4 Hz, H^4, H^8), 7.41 (2H, s, NH_2), 7.28 (2H, dt, J 11.6, 1.4 Hz, H^5, H^7), 4.35 (4H, q, J 7.1 Hz, CH_2), 1.37 (6H, t, J 7.1 Hz, CH_3) ppm; δ_C (125 MHz, $(CD_3)_2SO$) 165.6, 163.8, 158.6, 139.9, 131.9, 121.4, 98.6, 59.2, 14.5 ppm; IR ν_{max} (film) 3499, 3353, 3243, 2959, 2925, 1660, 1636, 1580, 1536, 1508, 1491, 1416, 1383, 1354, 1327, 1262, 1197, 1166, 1100, 1025, 955, 908, 848, 803, 790, 745, 718, 692 cm^{-1}; HRMS (ESI+) m/z calcd for $(C_{16}H_{17}NO_5+Na)^+$, 326.0999; found 326.0996.

ASSOCIATED CONTENT

Supporting Information

The Supporting Information is available free of charge at https://pubs.acs.org/doi/10.1021/jacs.9b09813.

Synthetic procedures for **1**; procedures for preparation of ROS in Figures 4, 6, and 7; computational data for **1** and **2**; spectroscopic and crystallographic data for **2**; procedures for two-photon fluorescence imaging; supplemental figures and tables (PDF)

AUTHOR INFORMATION

Corresponding Authors

*kimhm@ajou.ac.kr
*t.d.james@bath.ac.uk
*s.e.lewis@bath.ac.uk

ORCID

Maria Weber: 0000-0002-7492-1035
Carlos M. Lopez-Alled: 0000-0002-8117-4971
Claire L. McMullin: 0000-0002-4924-2890
Gabriele Kociok-Köhn: 0000-0002-7186-1399
Jannis Wenk: 0000-0001-9182-0407
Steven D. Bull: 0000-0001-8244-5123
Juyoung Yoon: 0000-0002-1728-3970
Hwan Myung Kim: 0000-0002-4112-9009
Tony D. James: 0000-0002-4095-2191
Simon E. Lewis: 0000-0003-4555-4907

DOI: 10.1021/jacs.9b09813
J. Am. Chem. Soc. 2019, 141, 19389–19396

Author Contributions

[#]L.C.M., M.W., S.J.P., and W.T.K. contributed equally.

Notes

The authors declare no competing financial interest.

■ ACKNOWLEDGMENTS

We are grateful for Ph.D. funding to C.M.L.-A. from the EU Horizon 2020 research and innovation program under Grant Agreement H2020-MSCA-CO-FUND, No. 665992. We thank the Center for Doctoral Training in Sustainable Chemical Technologies for Ph.D. funding to M.W. under EPSRC Grant EP/L016354/1. We also thank EPSRC for DTP Ph.D. funding to L.C.M. H.M.K. acknowledges a grant from the National Leading Research Lab Program of the National Research Foundation of Korea (NRF), funded by the Korean government (MSIP; No. 2016R1E1A1A02920873). In addition, T.D.J. wishes to thank the Royal Society for a Wolfson Research Merit Award and for funding to F.P.-C. under Grant CHG\R1\170010. This work was supported by a seed corn grant from the CR@B (Cancer Research at Bath) network. The British-Spanish Society and Plastic Energy are thanked for a 2017 Scholarship to C. M. L.-A. This research made use of the Balena High Performance Computing (HPC) Service at the University of Bath. NMR, X-ray crystallography, and MS facilities were provided through the Materials and Chemical Characterisation Facility (MC^2) at the University of Bath. We thank Prof. Uwe Pischel and Prof. Thorfinnur Gunnlaugsson for helpful discussions.

■ REFERENCES

(1) (a) Adams, L.; Franco, M. C.; Estevez, A. G. Reactive nitrogen species in cellular signaling. *Exp. Biol. Med.* **2015**, *240*, 711−717. (b) Dickinson, B. C.; Chang, C. J. Chemistry and biology of reactive oxygen species in signaling or stress responses. *Nat. Chem. Biol.* **2011**, *7*, 504−511. (c) Bove, P. F.; van der Vliet, A. Nitric oxide and reactive nitrogen species in airway epithelial signaling and inflammation. *Free Radical Biol. Med.* **2006**, *41*, 515−527. (d) Nathan, C. Specificity of a third kind: reactive oxygen and nitrogen intermediates in cell signaling. *J. Clin. Invest.* **2003**, *111*, 769−778.

(2) (a) Veal, E. A.; Day, A. M.; Morgan, B. A. Hydrogen peroxide sensing and signaling. *Mol. Cell* **2007**, *26*, 1−14. (b) Finkel, T.; Serrano, M.; Blasco, M. A. The common biology of cancer and aging. *Nature* **2007**, *448*, 767−774. (c) Barnham, K. J.; Masters, C. L.; Bush, A. I. Neurodegenerative diseases and oxidative stress. *Nat. Rev. Drug Discovery* **2004**, *3*, 205−214.

(3) (a) Kaur, H.; Halliwell, B. Evidence for nitric oxide-mediated oxidative damage in chronic inflammation. Nitrotyrosine in serum and synovial fluid from rheumatoid patients. *FEBS Lett.* **1994**, *350*, 9−12. (b) Dean, R. T.; Fu, S.; Stocker, R.; Davies, M. J. Biochemistry and pathology of radical-mediated protein oxidation. *Biochem. J.* **1997**, *324*, 1−18. (c) Kawasaki, H.; Ikeda, K.; Shigenaga, A.; Baba, T.; Takamori, K.; Ogawa, H.; Yamakura, F. Mass spectrometric identification of tryptophan nitration sites on proteins in peroxynitrite-treated lysates from PC12 cells. *Free Radical Biol. Med.* **2011**, *50*, 419−427.

(4) (a) Pacher, P.; Beckman, J. S.; Liaudet, L. Nitric oxide and peroxynitrite in health and disease. *Physiol. Rev.* **2007**, *87*, 315−424. (b) Kossenjans, W.; Eis, A.; Sahay, R.; Brochman, D.; Myatt, L. Role of peroxynitrite in altered fetal-placental vascular reactivity in diabetes or preeclampsia. *Am. J. Physiol.: Heart Circ. Physiol.* **2000**, *278*, 1311−1319. (c) Schieke, S. M.; Briviba, K.; Klotz, L. O.; Sies, H. Activation pattern of mitogen-activated protein kinases elicited by peroxynitrite: attenuation by selenite supplementation. *FEBS Lett.* **1999**, *448*, 301−303. (d) Beckman, J. S.; Carson, M.; Smith, C. D.; Koppenol, W. H. ALS, SOD and peroxynitrite. *Nature* **1993**, *364*, 584−585.

(5) Chan, J.; Dodani, S. C.; Chang, C. J. Reaction-based small-molecule fluorescent probes for chemoselective bioimaging. *Nat. Chem.* **2012**, *4*, 973−984.

(6) For reviews, see: (a) Kwon, N.; Hu, Y.; Yoon, J. Fluorescent chemosensors for various analytes including reactive oxygen species, biothiol, metal ions, and toxic gases. *ACS Omega* **2018**, *3*, 13731−13751. (b) Chen, X.; Wang, F.; Hyun, J.; Wei, Y. T.; Qiang, J.; Ren, X.; Shin, I.; Yoon, J. Recent progress in the development of fluorescent, luminescent and colorimetric probes for detection of reactive oxygen and nitrogen species. *Chem. Soc. Rev.* **2016**, *45*, 2976−3016. (c) Chen, X.; Tian, X.; Shin, I.; Yoon, J. Fluorescent and luminescent probes for detection of reactive oxygen and nitrogen species. *Chem. Soc. Rev.* **2011**, *40*, 4783−4804. (d) Dickinson, B. C.; Srikun, D.; Chang, C. J. Mitochondrial-targeted fluorescent probes for reactive oxygen species. *Curr. Opin. Chem. Biol.* **2010**, *14*, 50−56. (e) Nagano, T. Bioimaging of nitric oxide. *Chem. Rev.* **2002**, *102*, 1235−1269.

(7) For reviews, see: (a) Lin, V. S.; Dickinson, B. C.; Chang, C. J. Boronate-based fluorescent probes: imaging hydrogen peroxide in living systems. *Methods Enzymol.* **2013**, *526*, 19−43. (b) Rhee, S. G.; Chang, T.-S.; Jeong, W.; Kang, D. Methods for detection and measurement of hydrogen peroxide inside and outside of cells. *Mol. Cells* **2010**, *29*, 539−549.

(8) For reviews, see: (a) Wang, S.; Chen, L.; Jangili, P.; Sharma, A.; Li, W.; Hou, J.-T.; Qin, C.; Yoon, J.; Kim, J. S. Design and applications of fluorescent detectors for peroxynitrite. *Coord. Chem. Rev.* **2018**, *374*, 36−54. (b) Prolo, C.; Rios, N.; Piacenza, L.; Álvarez, M. N.; Radi, R. Fluorescence and chemiluminescence approaches for peroxynitrite detection. *Free Radical Biol. Med.* **2018**, *128*, 59−68. (c) McQuade, L. E.; Lippard, S. J. Fluorescent probes to investigate nitric oxide and other reactive nitrogen species in biology. *Curr. Opin. Chem. Biol.* **2010**, *14*, 43−49.

(9) Denk, W.; Strickler, J. H.; Webb, W. W. Two-photon laser scanning fluorescence microscopy. *Science* **1990**, *248*, 73−76.

(10) Weissleder, R. A clearer vision for *in vivo* imaging. *Nat. Biotechnol.* **2001**, *19*, 316−317.

(11) Zipfel, W. R.; Williams, R. M.; Christie, R.; Nikitin, A. Y.; Hyman, B. T.; Webb, W. W. Live tissue intrinsic emission microscopy using multiphoton-excited native fluorescence and second harmonic generation. *Proc. Natl. Acad. Sci. U. S. A.* **2003**, *100*, 7075−7080.

(12) For reviews, see: (a) Kim, H. M.; Cho, B. R. Small-molecule two-photon probes for bioimaging applications. *Chem. Rev.* **2015**, *115*, 5014−5055. (b) Yao, S.; Belfield, K. D. Two-photon fluorescent probes for bio-imaging. *Eur. J. Org. Chem.* **2012**, *2012*, 3199−3217.

(13) Jou, M. J.; Jou, S. B.; Guo, M. J.; Wu, H. Y.; Peng, T. I. Mitochondrial reactive oxygen species generation and calcium increase induced by visible light in astrocytes. *Ann. N. Y. Acad. Sci.* **2004**, *1011*, 45−56.

(14) (a) Li, H.; Yao, Q.; Fan, J.; Du, J.; Wang, J.; Peng, X. A two-photon NIR-to-NIR fluorescent probe for imaging hydrogen peroxide in living cells. *Biosens. Bioelectron.* **2017**, *94*, 536−543. (b) Zhao, W.; Li, Y.; Yang, S.; Chen, Y.; Zheng, J.; Liu, C.; Qing, Z.; Li, J.; Yang, R. Target-activated modulation of dual-color and two-photon fluorescence of graphene quantum dots for *in vivo* imaging of hydrogen peroxide. *Anal. Chem.* **2016**, *88*, 4833−4840. (c) Ahn, H.-Y.; Fairfull-Smith, K. E.; Morrow, B. J.; Lussini, V.; Kim, B.; Bondar, M. V.; Bottle, S. E.; Belfield, K. D. Two-photon fluorescence microscopy imaging of cellular oxidative stress using profluorescent nitroxides. *J. Am. Chem. Soc.* **2012**, *134*, 4721−4730. (d) Dong, B.; Song, X.; Kong, X.; Wang, C.; Tang, Y.; Liu, Y.; Lin, W. Simultaneous near-infrared and two-photon *in vivo* imaging of H_2O_2 using a ratiometric fluorescent probe based on the unique oxidative rearrangement of oxonium. *Adv. Mater.* **2016**, *28*, 8755−8759. (e) Zhang, K.-M.; Dou, W.; Li, P.-X.; Shen, R.; Ru, J.-X.; Liu, W.; Cui, Y.-M.; Chen, C.-Y.; Liu, W.-S.; Bai, D.-C. A coumarin-based two-photon probe for hydrogen peroxide. *Biosens. Bioelectron.* **2015**, *64*, 542−546.

(15) (a) Lee, D.; Lim, C. S.; Ko, G.; Kim, D.; Cho, M. K.; Nam, S.-J.; Kim, H. M.; Yoon, J. A Two-photon fluorescent probe for imaging endogenous $ONOO^-$ near NMDA receptors in neuronal cells and

DOI: 10.1021/jacs.9b09813
J. Am. Chem. Soc. 2019, 141, 19389−19396

hippocampal tissues. *Anal. Chem.* **2018**, *90*, 9347−9352. (b) Li, X.; Tao, R.-R.; Hong, L.-J.; Cheng, J.; Jiang, Q.; Lu, Y.-M.; Liao, M.-H.; Ye, W.-F.; Lu, N.-N.; Han, F.; Hu, Y.-Z.; Hu, Y.-H. Visualizing peroxynitrite fluxes in endothelial cells reveals the dynamic progression of brain vascular injury. *J. Am. Chem. Soc.* **2015**, *137*, 12296−12303. (c) Xie, X.; Tang, F.; Liu, G.; Li, Y.; Su, X.; Jiao, X.; Wang, X.; Tang, B. Mitochondrial peroxynitrite mediation of anthracycline-induced cardiotoxicity as visualized by a two-photon near-infrared fluorescent probe. *Anal. Chem.* **2018**, *90*, 11629−11635. (d) Sun, C.; Du, W.; Wang, P.; Wu, Y.; Wang, B.; Wang, J.; Xie, W. A novel mitochondria-targeted two-photon fluorescent probe for dynamic and reversible detection of the redox cycles between peroxynitrite and glutathione. *Biochem. Biophys. Res. Commun.* **2017**, *494*, 518−525. (e) Sun, W.; Shi, Y.-D.; Ding, A.-X.; Tan, Z.-L; Chen, H.; Liu, R.; Wang, R.; Lu, Z.-L. Imaging viscosity and peroxynitrite by a mitochondria-targeting two-photon ratiometric fluorescent probe. *Sens. Actuators, B* **2018**, *276*, 238−246. (f) Cheng, D.; Pan, Y.; Wang, L.; Zeng, Z.; Yuan, L.; Zhang, X.; Chang, Y.-T. Selective visualization of the endogenous peroxynitrite in an inflamed mouse model by a mitochondria-targetable two-photon ratiometric fluorescent probe. *J. Am. Chem. Soc.* **2017**, *139*, 285−292.

(16) For reviews, see: (a) Abou-Hadeed, K.; Hansen, H.-J. Product subclass 4: Azulenes and benzazulenes. *Sci. Synth* **2010**, *45*, 1060. (b) Hansen, H.-J. Birth of a structure. The 60th anniversary of the establishment of the azulene formula by Pfau and Plattner. Part 2. *Chimia* **1997**, *51*, 147. (c) Hansen, H.-J. Birth of a structure. The 60th anniversary of the establishment of the azulene formula by Pfau and Plattner. Part 1. *Chimia* **1996**, *50*, 489. (d) Lloyd, D. *The Chemistry of Conjugated Cyclic Compounds*; Wiley: Chichester, U.K., 1989; Chapter 13. (e) *Carbocyclic π-Electron Systems*; Kropf, H., Ed.; Georg Thieme: Stuttgart, 1985; Vol. V/2c, p 127. (f) Lloyd, D. *Nonbenzenoid Conjugated Carbocyclic Compounds*; Elsevier: Amsterdam, 1984; pp 352−377. (g) Mochalin, V. B.; Porshnev, Y. N. Advances in the chemistry of azulene. *Russ. Chem. Rev.* **1977**, *46*, 530.

(17) Bearpark, M. J.; Bernardi, F.; Clifford, S.; Olivucci, M.; Robb, M. A.; Smith, B. R.; Vreven, T. The Azulene S_1 state decays via a conical intersection: A CASSCF study with MMVB dynamics. *J. Am. Chem. Soc.* **1996**, *118*, 169−175.

(18) (a) Wagner, B. D.; Tittelbach-Helmrich, D.; Steer, R. P. Radiationless decay of the S_2 states of azulene and related compounds: Solvent dependence and the energy gap law. *J. Phys. Chem.* **1992**, *96*, 7904−7908. (b) Griesser, H. J.; Wild, U. P. The energy gap dependence of the radiationless transition rates in azulene and its derivatives. *Chem. Phys.* **1980**, *52*, 117−131. (c) Murata, S.; Iwanaga, C.; Toda, T.; Kokubun, H. Fluorescence yields of azulene derivatives. *Chem. Phys. Lett.* **1972**, *13*, 101−104 *erratum*, **1972**, *15*, 152.

(19) Beer, M.; Longuet-Higgins, H. C. Anomalous light emission of azulene. *J. Chem. Phys.* **1955**, *23*, 1390−1391.

(20) Kasha, M. Characterization of electronic transitions in complex molecules. *Discuss. Faraday Soc.* **1950**, *9*, 14−19.

(21) Itoh, T. Fluorescence and phosphorescence from higher excited states of organic molecules. *Chem. Rev.* **2012**, *112*, 4541−4568.

(22) For selected recent examples, see: (a) Gao, H.; Ge, C.; Hou, B.; Xin, H.; Gao, X. Incorporation of 1,3-free-2,6-connected azulene units into the backbone of conjugated polymers: Improving proton responsiveness and electrical conductivity. *ACS Macro Lett.* **2019**, *8*, 1360−1364. (b) Xin, H.; Li, J.; Yang, X.; Gao, X. Azulene-based BN-heteroaromatics. *J. Org. Chem.* **2019**, DOI: 10.1021/acs.joc.9b01724. (c) Murfin, L. C.; López-Alled, C. M.; Sedgwick, A. C.; Wenk, J.; James, T. D.; Lewis, S. E. A simple, azulene-based colorimetric probe for the detection of nitrite in water. *Front. Chem. Sci. Eng.* **2019**, DOI: 10.1007/s11705-019-1790-7. (d) Tang, T.; Lin, T.; Erden, F.; Wang, F. K.; He, C. Configuration-dependent optical properties and acid susceptibility of azulene compounds. *J. Mater. Chem. C* **2018**, *6*, 5153−5160. (e) Lichosyt, D.; Wasiłek, S.; Dydio, P.; Jurczak, J. The Influence of binding site geometry on anion-binding selectivity: A Case study of macrocyclic receptors built on the azulene skeleton. *Chem. - Eur. J.* **2018**, *24*, 11683−11692. (f) Buica, G.-O.; Lazar, I.-G.; Birzan, L.; Lete, C.; Prodana, M.; Enachescu, M.; Tecuceanu, V.; Stoian, A. B.; Ungureanu, E.-M. Azulene-ethylenediaminetetraacetic acid: A versatile molecule for colorimetric and electrochemical sensors for metal ions. *Electrochim. Acta* **2018**, *263*, 382−390. (g) López-Alled, C. M.; Sanchez-Fernandez, A.; Edler, K. J.; Sedgwick, A. C.; Bull, S. D.; McMullin, C. L.; Kociok-Köhn, G.; James, T. D.; Wenk, J.; Lewis, S. E. Azulene-boronate esters: colorimetric indicators for fluoride in drinking water. *Chem. Commun.* **2017**, *53*, 12580−12583. (h) Birzan, L.; Cristea, M.; Draghici, C. C.; Tecuceanu, V.; Maganu, M.; Hanganu, A.; Arnold, G.-L.; Ungureanu, E.-M.; Razus, A. C. 1-vinylazulenes - potential host molecules in ligands for metal ion detectors. *Tetrahedron* **2016**, *72*, 2316−2326. (i) Wakabayashi, S.; Uchida, M.; Tanaka, R.; Habata, Y.; Shimizu, M. Synthesis of azulene derivatives that have an azathiacrown ether moiety and their selective color reaction towards silver ions. *Asian J. Org. Chem.* **2013**, *2*, 786−791.

(23) For selected examples, see: (a) Zhou, Y.; Baryshnikov, G.; Li, X.; Zhu, M.; Ågren, H.; Zhu, L. Anti-Kasha's rule emissive switching induced by intermolecular H-bonding. *Chem. Mater.* **2018**, *30*, 8008−8016. (b) Gao, H.; Yang, X.; Xin, H.; Gao, T.; Gong, H.; Gao, X. Design, synthesis and properties of 2/6-aryl substituted azulene derivatives. *Youji Huaxue* **2018**, *38*, 2680−2692. (c) Gosavi, P. M.; Moroz, Y. S.; Korendovych, I. V. β-(1-Azulenyl)-L-alanine - A functional probe for determination of pKa of histidine residues. *Chem. Commun.* **2015**, *51*, 5347−5350. (d) Moroz, Y. S.; Binder, W.; Nygren, P.; Caputo, G. A.; Korendovych, I. V. Painting proteins blue: β-(1-azulenyl)-L-alanine as a probe for studying protein-protein interactions. *Chem. Commun.* **2013**, *49*, 490−492. (e) Koch, M.; Blacque, O.; Venkatesan, K. Impact of 2,6-connectivity in azulene: Optical properties and stimuli responsive behavior. *J. Mater. Chem. C* **2013**, *1*, 7400−7408. (f) Koch, M.; Blacque, O.; Venkatesan, K. Syntheses and tunable emission properties of 2-alkynyl azulenes. *Org. Lett.* **2012**, *14*, 1580−1583. (g) Salman, H.; Abraham, Y.; Tal, S.; Meltzman, S.; Kapon, M.; Tessler, N.; Speiser, S.; Eichen, Y. 1,3-Di(2-pyrrolyl)azulene: An efficient luminescent probe for fluoride. *Eur. J. Org. Chem.* **2005**, *2005*, 2207−2212. (h) Mazzuca, C.; Stella, L.; Venanzi, M.; Formaggio, F.; Toniolo, C.; Pispisa, B. Mechanism of membrane activity of the antibiotic trichogin GA IV: A two-state transition controlled by peptide concentration. *Biophys. J.* **2005**, *88*, 3411−3421. (i) Loidl, G.; Musiol, H.-J.; Budisa, N.; Huber, R.; Poirot, S.; Fourmy, D.; Moroder, L. Synthesis of β-(1-azulenyl)-L-alanine as a potential blue-colored fluorescent tryptophan analog and its use in peptide synthesis. *J. Pept. Sci.* **2000**, *6*, 139−144.

(24) Zhang, J.; Petoud, S. Azulene-moiety-based ligand for the efficient sensitization of four near-infrared luminescent lanthanide cations: Nd^{3+}, Er^{3+}, Tm^{3+}, and Yb3^{+}. *Chem. - Eur. J.* **2008**, *14*, 1264−1272.

(25) (a) Koh, C. J.; Lee, M. Fluorescence lifetime imaging microscopy of amyloid aggregates. *Bull. Korean Chem. Soc.* **2006**, *27*, 477−478. (b) Pham, W.; Weissleder, R.; Tung, C.-H. An azulene dimer as a near-infrared quencher. *Angew. Chem., Int. Ed.* **2002**, *41*, 3659−3662. (c) Lynch, D. E.; Hamilton, D. G. The history of azulenyl squaraines. *Aust. J. Chem.* **2017**, *70*, 857−871.

(26) (a) Zhou, Y.; Zhu, L. Involving synergy of green light and acidic responses in control of unimolecular multicolor luminescence. *Chem. - Eur. J.* **2018**, *24*, 10306−10309. (b) Zhou, Y.; Zou, Q.; Qiu, J.; Wang, L.; Zhu, L. Rational design of a green-light-mediated unimolecular platform for fast switchable acidic sensing. *J. Phys. Chem. Lett.* **2018**, *9*, 550−556. (c) Zhou, Y.; Zhuang, Y.; Li, X.; Ågren, H.; Yu, L.; Ding, J.; Zhu, L. Selective dual-channel imaging on cyanostyryl-modified azulene systems with unimolecularly tunable visible-near infrared luminescence. *Chem. - Eur. J.* **2017**, *23*, 7642−7647. (d) Dragu, E. A.; Ion, A. E.; Shova, S.; Bala, D.; Mihailciuc, C.; Voicescu, M.; Ionescu, S.; Nica, S. Visible-light triggered photoswitching systems based on fluorescent azulenyl-substituted dithienylcyclopentenes. *RSC Adv.* **2015**, *5*, 63282−63286. (e) Kitai, J.-i.; Kobayashi, T.; Uchida, W.; Hatakeyama, M.; Yokojima, S.; Nakamura, S.; Uchida, K. Photochromism of a diarylethene having an azulene ring. *J. Org. Chem.* **2012**, *77*, 3270−3276.

DOI: 10.1021/jacs.9b09813
J. Am. Chem. Soc. 2019, 141, 19389−19396

(27) (a) Cai, S.; Deng, W.; Huang, F.; Chen, L.; Tang, C.; He, W.; Long, S.; Li, R.; Tan, Z.; Liu, J.; Shi, J.; Liu, Z.; Xiao, Z.; Zhang, D.; Hong, W. Light-driven reversible intermolecular proton transfer at single-molecule junctions. *Angew. Chem., Int. Ed.* **2019**, *58*, 3829−3833. (b) Speiser, S. Prospects of luminescence based molecular scale logic gates and logic circuits. *J. Lumin.* **2016**, *169B*, 458−465. (c) Sangtarash, S.; Huang, C.; Sadeghi, H.; Sorohhov, G.; Hauser, J.; Wandlowski, T.; Hong, W.; Decurtins, S.; Liu, S.-X.; Lambert, C. J. Searching the hearts of graphene-like molecules for simplicity, sensitivity, and logic. *J. Am. Chem. Soc.* **2015**, *137*, 11425−11431. (d) Yeow, E. K. L.; Steer, R. P. Energy transfer involving higher electronic states: a new direction for molecular logic gates. *Chem. Phys. Lett.* **2003**, *377*, 391−398. (e) Remacle, F.; Speiser, S.; Levine, R. D. Intermolecular and intramolecular logic gates. *J. Phys. Chem. B* **2001**, *105*, 5589−5591.

(28) Nolting, D. D.; Nickels, M.; Tantawy, M. N.; Yu, J. Y. H.; Xie, J.; Peterson, T. E.; Crews, B. C.; Marnett, L.; Gore, J. C.; Pham, W. Convergent synthesis and evaluation of ^{18}F-labeled azulenic COX2 probes for cancer imaging. *Front. Oncol.* **2013**, *2*, 207.

(29) (a) Wurzer, A. J.; Wilhelm, T.; Piel, J.; Riedle, E. Comprehensive measurement of the S_1 azulene relaxation dynamics and observation of vibrational wavepacket motion. *Chem. Phys. Lett.* **1999**, *299*, 296−302. (b) Tran, P.; Meath, W. J.; Wagner, B. D.; Steer, R. P. Perturbative treatments of pump-probe laser-molecule interactions with applications to azulene and trimethylazulene. *J. Chem. Phys.* **1994**, *100*, 4165−4170. (c) Matsumoto, T.; Ueda, K.; Tomita, M. Femtosecond vibrational relaxation measurement of azulene using temporally incoherent light. *Chem. Phys. Lett.* **1992**, *191*, 627−632. (d) Schwarzer, D.; Troe, J.; Schroeder, J. S_1-Lifetime of azulene in solution. *Berich. Bunsen Gesell.* **1991**, *95*, 933−934. (e) Mitchell, D. R.; Gillispie, G. D. The $S_2 \leftarrow S_1$ absorbance spectrum of azulene determined by two-color two-photon fluorescence excitation. *J. Phys. Chem.* **1989**, *93*, 4390−4393. (f) Iyoda, T.; Sakamaki, K.; Shimidzu, T.; Honda, K. Two-photon energy-transfer-type sensitization of titanium dioxide single crystal electrode by azulene. *Proc. Electrochem. Soc.* **1988**, *88−14*, 169−175. (g) Wirth, P.; Schneider, S.; Doerr, F. Ultrafast electronic relaxation in the S_1 state of azulene and some of its derivatives. *Chem. Phys. Lett.* **1976**, *42*, 482−487. (h) Bergman, A.; Jortner, J. Consecutive two-photon absorption of azulene in solution utilizing dye lasers. *Chem. Phys. Lett.* **1973**, *20*, 8−10.

(30) (a) Koide, T.; Takesue, M.; Murafuji, T.; Satomi, K.; Suzuki, Y.; Kawamata, J.; Terai, K.; Suzuki, M.; Yamada, H.; Shiota, Y.; Yoshizawa, K.; Tani, F. An Azulene-fused tetracene diimide with a small HOMO-LUMO gap. *ChemPlusChem* **2017**, *82*, 1010−1014. (b) Kawamata, J.; Suzuki, Y. A novel molecular design strategy for efficient two-photon absorption materials. *Curr. Pharm. Biotechnol.* **2012**, *13*, 2569−2574. (c) Hirakawa, S.; Kawamata, J.; Suzuki, Y.; Tani, S.; Murafuji, T.; Kasatani, K.; Antonov, L.; Kamada, K.; Ohta, K. Two-photon absorption properties of azulenyl compounds having a conjugated ketone backbone. *J. Phys. Chem. A* **2008**, *112*, 5198−5207. (d) Kurotobi, K.; Suk Kim, K.; Noh, S. B.; Kim, D.; Osuka, A. A quadruply azulene-fused porphyrin with intense near-IR absorption and a large two-photon absorption cross section. *Angew. Chem., Int. Ed.* **2006**, *45*, 3944−3947.

(31) Ghazvini Zadeh, E. H.; Tang, S.; Woodward, A. W.; Liu, T.; Bondar, M. V.; Belfield, K. D. Chromophoric materials derived from a natural azulene: Syntheses, halochromism and one-photon and two-photon microlithography. *J. Mater. Chem. C* **2015**, *3*, 8495−8503.

(32) Woodward, A. W.; Ghazvini Zadeh, E. H.; Bondar, M. V.; Belfield, K. D. Computer aided chemical design: using quantum chemical calculations to predict properties of a series of halochromic guaiazulene derivatives. *R. Soc. Open Sci.* **2016**, *3*, 160373.

(33) (a) Takase, K.; Asao, T.; Takagi, Y.; Nozoe, T. Syntheses and some properties of 2- and 6-hydroxyazulenes. *Chem. Commun.* **1968**, 368−370. (b) Morita, T.; Kanzawa, H.; Takase, K. The synthesis and some properties of 2,6-dihydroxyazulene. *Chem. Lett.* **1977**, *6*, 753−756.

(34) (a) Nozoe, T.; Asao, T.; Susumago, H.; Ando, M. Diazotization of 2-aminoazulene derivatives. Formation of 2-diazo-2,6-azulenoquinone derivatives. *Bull. Chem. Soc. Jpn.* **1974**, *47*, 1471−1476. (b) Makosza, M.; Podraza, R. Hydroxylation and amination of azulenes by vicarious nucleophilic substitution of hydrogen. *Eur. J. Org. Chem.* **2000**, *2000*, 193−198.

(35) (a) Nolting, D. D.; Nickels, M.; Price, R.; Gore, J. C.; Pham, W. Synthesis of bicyclo[5.3.0]azulene derivatives. *Nat. Protoc.* **2009**, *4*, 1113−1117. (b) Nozoe, T.; Takase, K.; Kato, M.; Nogi, T. Reaction of 2-arylsulfonyloxytropones and active methylene compounds. Formation of 8-hydroxy-2H-cyclohepta[b]furan-2-one and 2-amino-8H-cyclohepta[b]furan-8-one derivatives. *Tetrahedron* **1971**, *27*, 6023−6035. (c) Holovics, T. C.; Robinson, R. E.; Weintrob, E. C.; Toriyama, M.; Lushington, G. H.; Barybin, M. V. The 2,6-Diisocyanoazulene motif: Synthesis and efficient mono- and heterobimetallic complexation with controlled orientation of the azulenic dipole. *J. Am. Chem. Soc.* **2006**, *128*, 2300−2309. (d) Kurotobi, K.; Tabata, H.; Miyauchi, M.; Murafuji, T.; Sugihara, Y. Coupling reaction of azulenyl-4,4,5,5-tetramethyl-1,3,2-dioxaborolanes with haloazulenes. *Synthesis* **2002**, *2002*, 1013−1016.

(36) Sikora, A.; Zielonka, J.; Lopez, M.; Joseph, J.; Kalyanaraman, B. Direct oxidation of boronates by peroxynitrite: Mechanism and implications in fluorescence imaging of peroxynitrite. *Free Radical Biol. Med.* **2009**, *47*, 1401−1407.

(37) Xu, C.; Webb, W. W. Measurement of two-photon excitation cross sections of molecular fluorophores with data from 690 to 1050 nm. *J. Opt. Soc. Am. B* **1996**, *13*, 481−491.

(38) Tanabe, T.; Otani, H.; Mishima, K.; Ogawa, R.; Inagaki, C. Phorbol 12-myristate 13-acetate (PMA)-induced oxyradical production in rheumatoid synovial cells. *Jpn. J. Pharmacol.* **1997**, *73*, 347−351.

(39) Karabay, A. Z.; Koç, A.; Özkan, T.; Büyükbıngöl, Z.; Sunguroğlu, A.; Aktan, F. Effect of taurine on hydrogen peroxide production in lipopolisaccharide induced RAW264.7 macrophage cells. *FABAD J. Pharm. Sci.* **2008**, *33*, 187−192.

(40) (a) Feelisch, M.; Ostrowski, J.; Noack, E. On the mechanism of nitric oxide release from sydnonimines. *J. Cardiovasc. Pharmacol.* **1989**, *14*, S13−S22. (b) Lomonosova, E. E.; Kirsch, M.; Rauen, U.; de Groot, H. The critical role of Hepes in SIN-1 cytotoxicity, peroxynitrite versus hydrogen peroxide. *Free Radical Biol. Med.* **1998**, *24*, 522−528.

(41) (a) Yang, C. F.; Shen, H. M.; Ong, C. N. Protective effect of ebselen against hydrogen peroxide-induced cytotoxicity and DNA damage in HepG2 cells. *Biochem. Pharmacol.* **1999**, *57*, 273−279. (b) Daiber, A.; Zou, M. H.; Bachschmid, M.; Ullrich, V. Ebselen as a peroxynitrite scavenger *in vitro* and *ex vivo*. *Biochem. Pharmacol.* **2000**, *59*, 153−160.

DOI: 10.1021/jacs.9b09813
J. Am. Chem. Soc. 2019, 141, 19389−19396